Title
Geology of the Wilkes land sub-basin and stability of the East Antarctic Ice Sheet: Insights from rock magnetism at IODP Site U1361

Author
Tauxe, Lisa

Publication Date
2014-10-01

Peer reviewed

Geology of the Wilkes Land Sub-basin and Stability of the East Antarctic Ice Sheet: Insights from rock magnetism at IODP Site U1361

L. Tauxe[a,b], S. Sugisaki[a,c], F. Jiménez-Espejo[d], C. Escutia[e], C.P. Cook[f], T. van de Flierdt[g], M. Iwai[h]

[a] *Scripps Institution of Oceanography, La Jolla, CA, USA.*
[b] *ltauxe@ucsd.edu*
[c] *Department of Earth and Planetary Science University of Tokyo 7-3-1 Hongo Bunkyo-ku Tokyo 113-0033 Japan*
[d] *Department of Biogeochemistry, Japan Agency for Marine-Earth Science and Technology (JAMSTEC) 2-15 Natsushima, Yokosuka, 237-0061, Japan*
[e] *Instituto Andaluz de Ciencias de la Tierra CSIC-Univ Granada Av. de las Palmeras, 4 18100 Armilla (Granada) Spain*
[f] *Department of Geological Sciences, University of Florida, Gainesville, FL, USA.*
[g] *Department of Earth Science and Engineering Imperial College London SW7 2AZ London United Kingdom*
[h] *Department of Natural Environmental Science Kochi University 2-5-1 Akebono-cho Kochi 780-8520 Japan*

Abstract

IODP Expedition 318 drilled Site U1361 on the continental rise offshore of Adélie Land and the Wilkes sub-glacial basin. The objective was to reconstruct the stability of the East Antarctic Ice Sheet (EAIS) during Neogene warm periods, such as the late Miocene and the early Pliocene. The sedimentary record tells a complex story of compaction, and erosion (thus hiatuses). Teasing out the paleoenvironmental implications is essential for understanding the evolution of the EAIS. Anisotropy of magnetic susceptibility (AMS) is sensitive to differential compaction and other rock magnetic parameters like isothermal remanence and anhysteretic remanence are very sensitive to changes in the terrestrial source region. In general, highly anisotropic layers correspond with laminated clay-rich units, while more isotropic layers are bioturbated and have less clay. Layers enriched in diatoms are associated with the latter, which also have higher Ba/Al ratios consistent with higher productivity. Higher anisotropy layers have lower porosity and moisture contents and have fine grained magnetic mineralogy dominated by maghemite, the more oxidized form of iron oxide, while the lower anisotropy layers have magnetic mineralogies dominated by magnetite. The different magnetic mineralogies support the suggestion based on isotopic signatures by Cook et al. (2013) of different source regions during low productivity (cooler) and high productivity (warmer) times. These two facies were tied to the coastal outcrops of the Lower Paleozoic granitic terranes and the Ferrar Large Igneous Province in the more inland Wilkes Subglacial Basin respectively. Here we present evidence for a third geological unit, one eroded at the boundaries between the high and low clay zone with a "hard" (mostly hematite) dominated magnetic mineralogy. This unit likely outcrops in the Wilkes sub-glacial basin and could be hydrothermally altered Beacon sandstone similar to that detected by Craw and Findlay (1984) in Taylor Valley or the equivalent to the Elatina Formation in the Adelaide Geosyncline in Southern Australia (Schmidt and Williams, 2013). Correlation of the "hard" events with global oxygen isotope stacks of Zachos et al. (2001) and Lisiecki and Raymo (2005) suggest that the source region was eroded during times with higher global ice volume.

Keywords: East Antarctic Ice Sheet Stability, rock magnetism, Pliocene paleoclimate, Integrated Ocean Drilling Program, Joides Resolution, Expedition 318, Site U1361

1. Introduction

As atmospheric CO_2 levels exceed the 400 ppm mark, our eyes naturally turn to the last time they were that high, the Pliocene, when they were estimated to be between 365 and 415 ppm (Pagani et al., 2010). Implications for temperature and sea level rise can perhaps be gleaned by such comparisons. Global sea level is controlled by both temperature and the amount of ice stored on continents. As global climate changes, understanding the response of global ice volume to rising temperatures is urgently needed. For example, melting of the Greenland Ice sheet would result in a 7 m rise, and full deglaciation of the Western Antarctic Ice Sheet (WAIS) and East Antarctic Ice Sheet (EAIS) would contribute another ∼5 m and 52 m respectively (Lythe et al., 2001) (see also Fretwell et al. (2013)). Whereas it appears likely that the Greenland Ice Sheet is quite vulnerable to warming climate (Gregory et al., 2004), at least some studies (Huybrechts and de Wolde, 1999) predict that the EAIS will grow owing to increased precipitation (see also Alley et al. (2005)). Worryingly, recent reports indicate that while parts of the EAIS are growing, other parts are decreasing (Fig. 1 and Vaughan et al. (2013)). The past response of the EAIS in times with comparable tectonic configurations and atmospheric CO_2 levels to the present day, i.e. in the Pliocene, therefore are needed to inform current discussions of rising sea-levels. While Miller et al. (2012) summarized evidence for global sea-level that was 22 ±10 m higher than present during the Pliocene, concluding that is was "very likely that several meters of eustatic rise can be attributed to ice loss from the marine margins of East Antarctica.", the large error bars leave room for considerable doubt.

An attractive target for investigating EAIS stability is the eastern sector of the Wilkes Land margin, located at the seaward termination of the largest East Antarctic subglacial basin, the Wilkes subglacial basin on Wilkes Land, Antarctica (Fig. 1). Such an investigation was one of the rationales for the drilling of Site U1361 (64.2457°S, 143.5320°E) during Expedition 318 of the International Ocean Drilling Program (Escutia et al., 2011). In an initial study, Cook et al. (2013) reported strontium and neodymium isotopic ratios from detrital material indicating erosion of two distinctly different source bodies, now mostly under the ice sheet. They interpreted the data as evidence for retreat of the ice sheet margin several hundreds of kilometers inland during the warmer intervals of the Pliocene. Here we report complimentary rock magnetic data which provide additional evidence for their conclusions and point to erosion of a third geological unit accessed during glacial advance and retreat.

2. Material and Methods

Site U1361 was drilled into a submarine levee off the coast of Adélie Land, just to the west of the Wilkes subglacial basin. Hole U1361A was cored using the advanced piston coring system to refusal at 151.5 mbsf below which an extended core barrel was used to a depth of 388 mbsf. Tauxe et al. (2012) compiled magneto-, bio-, and lithostratigraphic information for the Expedition 318 cores documenting a sedimentary record from the Middle Miocene to the late Pleistocene with few hiatuses and excellent magnetostratigraphic control. The complete data set of previously published paleomagnetic and rock magnetic data is available in the MagIC database at: http://earthref.org/doi/10.1029/2012PA002308

The interval studied here is 40-160 mbsf and spans ∼2.2 Ma to 6.4 Ma (Fig. 2). Two major lithofacies are represented: laminated clay-rich units and bioturbated units with less clay and more abundant diatoms.

Paleomagnetic samples were taken every core section (∼ 1.5 m intervals) for a total of 80 discrete samples. Anisotropy of magnetic susceptibility (AMS) including bulk susceptibility (χ) was measured on all discrete samples on the Kappabridge KLY4S magnetic susceptibility instrument either on the ship or in the Scripps Paleomagnetic Laboratory. These data, represented as maximum, intermediate and minimum eigenvalues (τ_1, τ_2, τ_3) were reported by Tauxe et al. (2012). Shipboard measurements of moisture content, porosity, and natural gamma ray (NGR) were reported by Escutia et al. (2011). As part of the post-cruise geochemical investigations, Cook et al. (2013) measured x-ray fluorescence (XRF), diatom valve concentrations (DVC) and strontium and neodymium isotopes. The XRF data from Cook et al. (2013) are shown as black lines while those reported here are in blue. Here we use the barium/aluminum (Ba/Al) ratio and shipboard NGR (Escutia et al., 2011) as a proxies for primary productivity (Dymond et al., 1992) and the clay fraction (Dunlea et al., 2013) respectively in the cores.

For the present study, we measured anhysteretic remanence (ARM) acquired in an alternating field of 180 mT in the presence of a 50 μT DC bias field using an SI-4 alternating field demagnetizer and measured using the 2-G Enterprises magnetometer in the Scripps Paleomagnetic Laboratory. Following the ARM step, IRMs were imparted to the discrete samples using an ASC impulse demagnetizer in fields increasing up to ∼1.2 T. We refer here to the ratio of the IRM at 1 T and the 0.5 IRM steps as the $\mathrm{IRM}_{0.5T}^{1.0T}$ ratio. Following IRM acquisition experiments, small chips were taken from representative cubes and glued into clean glass vials with KaSil cement. These were exposed again to a field of ∼1 T along the (new) X direction. A second IRM was imparted in a 0.5 T field along the Y axis and a third IRM in a 0.1 T field along the Z axis. The specimens were then thermally demagnetized in a step-wise fashion to determine the blocking temperatures of the different coercivity fractions in the specimens in an experiment known as the '3D-IRM demagnetization experiment' of Lowrie (1990). All rock and paleomagnetic data analyzed for the present study are available for download from the MagIC data base at:

http://earthref.org/doi/10.1029/2012PA002308

Geochemical and physical property data used in the interpretations here are available for download from the ERDA along with the Python scripts used to generate the figures.

3. Results

3.1. Anisotropy of magnetic susceptibility

We re-plot the eigenvalues of the AMS tensors for the interval 40-160 mbsf from Hole U1361A as presented by Tauxe et al. (2012) in Fig. 2a. One measure of the degree of anisotropy is the ratio of τ_1/τ_3, usually termed P (Chapter 13 in Tauxe et al. (2010)), is shown in Fig. 2b. Stratigraphic intervals with high values of P (here taken as > 1.03) are shaded in grey. We also plot the (uncalibrated) aluminum and barium data from the XRF measurements of Cook et al. (2013) in Figs. 2c and d (black lines) and report new data for the interval below 104 mbsf here (shown in blue). These data suggest that the zones of high anisotropy correspond with zones of high aluminum which in turn is directly related to the clay content. This contention is supported by the variations in natural gamma radiation (NGR), shown in Fig. 2e, whereby zones of relatively high NGR ($>\sim 34$) with few exceptions correspond to high P and also high aluminum (clay). We assume in the following that the high P and high NGR intervals ($>\sim 34$) can be used as proxies for clay-rich zones in this study.

Schwehr et al. (2006) investigated the role of porosity and water content (related to compaction) in controlling the anisotropy fabric and found a strong correlation. They showed that changes in anisotropy degree can result from compaction disequilibria resulting from changes in lithology, for example from alternating between clay-rich and clay-poor layers, or from hiatuses. Here, we plot moisture content and porosity in Fig. 2f. The grey (high anisotropy) zones do appear to be associated with zones of low moisture and porosity, further supporting the connection between anisotropy, clay content and laminated versus bioturbated layers.

The ratio of barium to aluminum is a proxy for primary productivity (see also Fig. 2) is shown in Fig. 3b. Zones of high Ba/Al ratios are closely associated with the low anisotropy zones (white). Using Ba/Al as a proxy for productivity, we infer that the clay rich intervals are associated with lower productivity. To further explore this possibility, we plot diatom valve counts of Cook et al. (2013) in Fig. 3c. We see that the two zones of high diatom valve counts are also associated with high Ba/Al and low AMS anisotropy. The expanded section from 88 to 104 mbsf in Fig. 3e shows shipboard high resolution core photos with light and dark bands associated with the low and high anisotropy values respectively. Note that the contrast on the photos was increased to highlight the patterns. As there are only two zones with significant diatom valve counts, the Ba/Al where measured is a superior lithological tool for identifying zones of high productivity. While Ba/Al was not measured for the entire core, P and NGR were, hence these represents important proxies for primary productivity in this interval of Hole U1361A. We note here that because the Ba/Al ratio plot is quite similar to the aluminum plot shown in Fig. 2, that it is possible that the ratio is dominated by variability in aluminum rather than barium and merely reflects the clay content as opposed to productivity.

3.2. Isothermal remanence

Representative examples of the behavior of the U1361A sediments during the IRM acquisition and 3D-IRM demagnetization experiments are shown in Fig. 4. Figs. 4a and b show the behavior of a specimen whose IRM saturated by about 0.3 T impulse ($\mathrm{IRM}_{0.5T}^{1.0T}$ of ~ 1); it is also virtually completely demagnetized by between 575 and 600°C (Fig. 4b) consistent with a magnetite remanence. All such 'Type I' specimens ($N = 21$) belong to the "clay-poor", bioturbated, low anisotropy ($P < 1.03$) and high productivity, lithofacies (e.g., Fig. 5a). Specimens like the one shown in Figs. 4c and d also saturate in low impulse fields but display an change in slope in the medium and low coercivity fraction (Y and Z axes) between 300 and 425°C. Frequently, these did not completely demagnetize until about 625°C (Fig. 4d), suggestive of maghemite. All of these 'Type II' specimens ($N = 20$) had P values greater than 1.03 and belong to the "clay-rich" facies associated with the laminated, low productivity intervals (e.g., Fig. 5b). The specimen shown in Figs. 4d and e does not saturate even in an impulse field of over 1 T ($\mathrm{IRM}^{1.0T}_{0.5T} = 1.11$) and has 57% of the (total) remanence remaining after demagnetization to 600°C. This 'Type III' behavior is characteristic of hematite. Eleven of the 13 specimens displaying this behavior were found at the boundaries between the high and low P zones (e.g., Fig. 5c). The two exceptions were found bordering zones with high NGR values. One of these is also adjacent to a sampling gap and hiatus inferred from the magnetostratigraphic pattern. The fourth type of behavior is that shown in Figs. 4g and h whereby the IRM acquisition curve is quite 'hard' with $\mathrm{IRM}^{1.0T}_{0.5T}$ values of $\sim$1.07, but the specimens are virtually completely demagnetized by between 575 and 600°C. This 'Type IV' behavior is characteristic of multi-axial single domain magnetite (Tauxe et al., 2002). All of these specimens ($N = 3$) were also found at the boundaries between the high and low P zones (e.g., Fig. 5d). The average P value of the Types III and IV specimens was 1.03 ± 0.02 or transitional between the 'low' and 'high' anisotropy zones. Therefore, for the purposes of this study, we classify specimens as being 'soft' if their $\mathrm{IRM}^{1.0T}_{0.5T}$ values were less than 1.03.

4. Discussion

ARM, IRM and χ are sensitive to magnetic grain size (Maher and Thompson, 1999) and are frequently plotted against one another to detect changes in grain size or changes in provenance (Banerjee et al., 1981). In Fig. 6a we plot the mass normalized ARM against bulk susceptibility (χ) in and ARM against IRM acquired in a 1.2 T field in Fig. 6b. All of the magnetically hard specimens ($\mathrm{IRM}_{0.5T}^{1.0T} > 1.03$, plotted as red dots) cluster near the origin. The remaining, magnetically soft, specimens can be divided into two groups: those that are characterized by low P (Type I, or magnetite remanences) and those with high P (Type II, or maghemite remanences). The two types have distinct slopes consistent with their different mineralogies and point to different sources of the magnetic minerals. It is not surprising that the high P specimens, belonging to the laminated clay facies, appear to have finer magnetic grain sizes, based on the steeper slope of the ARM versus χ trend lines. We note however that the interpretation as to grain size of such data (e.g., King et al. (1983)) is based solely on magnetite and should be used with caution in this case as there is evidence of significant maghemitization of the high P specimens. Nonetheless, the data demonstrate that the high and low clay facies have markedly different magnetic mineralogies and apparently also magnetic grain sizes. Therefore, the two 'soft' types must have different sedimentological histories.

The rock magnetic results point to three distinct populations of magnetic mineralogies. Fig. 7 shows the clay proxy NGR and $\mathrm{IRM}_{0.5T}^{1.0T}$ plotted against stratigraphic depth. With few exceptions, the magnetically soft magnetite specimens (black dots) in the $\mathrm{IRM}_{0.5T}^{1.0T}$ profile, are associated with the clay-poor facies (low P, indicated by white zones), while the magnetically soft maghemite specimens (brown dots), are associated with the clay-rich (high P, indicated by grey zones) specimens. The horizontal lines mark the positions of the magnetically hard specimens (red dots), which with only two exceptions (indicated as dotted black lines) are found at the transitions between high and low clay in the NGR clay proxy data.

The origin of the two 'soft' groups can be understood in the light of the ϵNd (the deviation of measured ^{143}Nd/^{144}Nd ratios from the Chondritic Uniform Reservoir in parts per 10,000) and ^{87}Sr/^{86}Sr isotopic data of Cook et al. (2013), shown in Fig. 7d. The intervals of low ϵNd (less than the dashed red line plotted at $\epsilon\text{Nd} < -9.25$) and high ^{87}Sr/^{86}Sr are all associated with clay-rich intervals (NGR >34). These were deposited (and presumably eroded) during the low-productivity (cooler?) intervals. In contrast, the clay-poor intervals with NGR<34 are associated with high ϵNd and low ^{87}Sr/^{86}Sr values, deposited during the higher productivity (warmer?) intervals during the Pliocene. Cook et al. (2013) inferred different source regions based on the isotopic signatures of the detrital material and tied these two groups to Lower Paleozoic terranes and the Ferrar Large Igneous Province (FLIP) respectively (see Fig. 8). Based on the occurrences of these two rock types on Wilkes Land, they argued that the cooler intervals have isotopic signatures compatible with granitic bedrock in the hinterland of the nearby Ninnis Glacier (NG on Fig.8). The warmer intervals have isotopic signatures like those of the FLIP rocks whose magnetic anomaly signature was detected in the Wilkes subglacial basin by Ferraccioli et al. (2009).

As already mentioned, with two exceptions, the high $\text{IRM}^{1.0T}_{0.5T}$ intervals (Types III and IV) are observed at the transitions between high and low NGR. All but three of these specimens are identifiable as hematite dominated. Hematite is unusual in such a grey-black sediments and is likely of detrital origin. Although glacial to interglacial transitions could be associated with changes in ventilation that can promote diagenetic enrichments involving secondary hematite pigmentation, reddish tinted horizons are not associated with the horizons actually sampled (e.g., Fig. 5c). Therefore, we suspect a third, as yet unidentified, terrane that eroded during glacial advance and retreat. The closest red bed units in outcrop (which could provide hematite rich sedimentary particles) appear to be Permian red beds of the Amery Group, exposed in the Prince Charles Mountains (see Mikhalsky et al. (2001), Keating and Sakai (1991) and references therein); these are quite distant from U1361 and are unlikely to be a source for the detrital hematite found at Site U1361. However, Veevers and Saeed (2011) found references to red sandstones in Mawson (1915) (v. 2, p 294). According to that delightful account,

> "Stillwell met with a great range of minerals and rocks in the terminal moraine near Winter Quarters, Adelie Land. Amongst them was red sandstone in abundance, suggesting that the Beacon sandstone formation extend also throughout Adelie Land, but is hidden by the ice-cap."

Moreover, Craw and Findlay (1984) found hydrothermally altered granitoids and Beacon sandstone with enrichment of hematite, altered by the intrusion of the Ferrar sills near Taylor Glacier. These units are also likely to occur in the Wilkes sub-glacial basin along with the FLIP units detected by Ferraccioli et al. (2009). Another likely source, however, is the Neoproterozoic Elatina Formation, exposed on the southern Australian margin in the Adelaide geosyncline Williams et al. (2008). This formation has recently been studied by Schmidt and Williams (2013) who found a remanence dominated by hematite. Aitken et al. (2014) reconstructed the geological connections between Australia and Antarctica largely based on magnetic and gravity anomalies. We show their reconstruction for the time prior to the break up of Gondwana at 160 Ma, along with the Adelaide basin (from Schmidt and Williams (2013) and Williams et al. (2008)) and the location of Site U1361 in Fig. 8 in present coordinates with respect to Antarctica. The Adelaide basin along with its hematite rich red beds are thought to correlate to units now covered by ice and have therefore not been identified in outcrop on the Antarctic margin. Notably, Finn et al. (2006) explained lows in the magnetic anomalies east of the Mawson block (MB in Fig. 8) as 'magnetite-poor upper Neoproterozoic and lower Paleozoic sedimentary rocks and their metamorphic equivalents'. It seems likely that there is a small outcrop of either Beacon red sandstone (as suspected by Mawson) or Elatina equivalent Neoproterozoic red beds on the Antarctic margin (Finn et al., 2006), that eroded during growth and decay of the East Antarctic Ice Sheet.

The Type IV behavior suggests a magnetically hard, magnetite remanence and the source of this phase is more elusive. Nonetheless, magnetically hard magnetite was frequently observed in the McMurdo volcanic province (see data of Lawrence et al. (2009) shown in Fig. 9) and McMurdo volcanics hidden under the ice sheet is also a possible source for such specimens. These would be difficult to distinguish from the FLIP units in aeromagnetic surveys.

The excellent magnetostratigraphic control for Site U1361 allows us to tie the hard $\mathrm{IRM}_{0.5T}^{1.0T}$ layers to the GPTS with a high degree of confidence (dashed green lines in Fig. 7). Patterson et al. (2014) performed a detailed and quantitative correlation of the interval of U1361A between 50 and 100 mbsf and we will not duplicate that effort here. Nonetheless, the oxygen isotopic stacks of Zachos et al. (2001) and Lisiecki and Raymo (2005) (black and red curves in Fig. 7e respectively with the cyan curve representing a low pass filtered version of the Zachos et al. (2001) data) are particularly intriguing here. While it is tempting but perhaps dangerous to tie a particular high $\mathrm{IRM}_{0.5T}^{1.0T}$ event to a particular isotopic event (say M2), it does appear likely that unusually cold intervals (high global δ^{18}O data in the filtered record between ∼5.6-6.2 Ma, 4.6-5 Ma and <3.6 Ma), result in erosion of an elusive hematite bearing lithofacies now hidden under the ice on Antarctic continent.

5. Conclusions

- Anisotropy of magnetic susceptibility is a sensitive indicator of the clay fraction at Hole U1361A. The clay-rich, high anisotropy, zones are apparently lower productivity and are likely associated with colder intervals while the clay-poor, low anisotropy, zones are associated with warmer intervals during the Pliocene.

- There are four distinct categories of behavior during IRM acquisition and thermal demagnetization. The first two (Types I and II) are magnetically 'soft' and are likely to be magnetite and its more oxidized cousin, maghemite. The second two (Types III and IV) are magnetically 'hard' and are likely to be hematite and a rare, magnetically hard, form of magnetite.

- The maghemite (Type II) mineralogies are associated with the clay-rich facies while the magnetite (Type I) remanences are associated with the clay-poor facies. In turn, these are associated with zones inferred to be lower and higher productivity, based on the Ba/Al ratios in the sediments hence belong to the colder and warmer intervals of the Pliocene respectively. These are also tied to the Paleozoic and Ferrar Large Igneous Province sources respectively according to the ϵNd and strontium isotopic results of Cook et al. (2013).

- The magnetically hard Types III and IV remanences (hematite and a few rare magnetite specimens respectively) are associated with the transition zones between clay poor and clay-rich facies. These were sourced in an unknown lithologic unit that eroded during glacial advance and retreat. It appears likely that the source for the hematite rich layers is either hydrothermally altered Beacon sandstone units or Neoproterozoic red beds, correlative to units in the Adelaide Basin studied by Schmidt and Williams (2013). The 'hard' magnetite layers could have a source in McMurdo volcanics. Both of these are likely hidden under the ice.

- The occurrence of the hard $\mathrm{IRM}_{0.5T}^{1.0T}$ layers in periods with more global ice volume is consistent with the contention that they are sourced in a geological unit that gets eroded during ice sheet advance and retreat of glaciers associated with particularly cold intervals.

- This study, in combination with the work of Cook et al. (2013), strongly supports an active response of the East Antarctic Ice Sheet to climatic forcing in the Pliocene. As CO_2 levels approach those last seen in the

Pliocene, we can expect a greater role of EAIS melting than is presently envisioned.

6. Acknowledgements

We acknowledge all the hard work by the shipboard scientific party (Stickley, C.E., Bijl, P.K., Bohaty, S., Brinkhuis, H., McKay, R., Passchier, S., Pross, J., Riesselman, C., Röhl, U., Welsh, K., Klaus, A., Fehr, A., Bendle, J.A.P. , Carr, S.A., Dunbar, R., Gonzàlez, J., Hayden, T., Katsuki, K., Kong, G.S., Nakai, M., Olney, M.P., Pekar, S.F., Sakai, T., Shrivastava, P.K., Tuo, S., Williams, T., Yamane, M.) and the crew aboard the JOIDES Resolution for making all things possible. In particular, we wish to thank Maggie Hastedt whose tireless and cheerful help in the paleomagnetic laboratory was essential to the success of our investigations. We also thank Jason Steindorf for making many of the measurements. This research used samples and data provided by the Integrated Ocean Drilling Program (IODP). Funding for this research was provided by National Science Foundation grants OCE1058858 and EAR1141840 to LT. We also acknowledge support of Spanish Ministry of Science Grant CTM2011-24079 to CE.

References

Aitken, A., Young, D., Ferraccioli, F., Betts, P., Greenbaum, J., Richter, T., Roberts, J., Blankenship, D., Siegert, M., 2014. The subglacial geology of Wilkes Land, East Antarctica. Geophys. Res. Lett. 41, 2390–2400.

Alley, R., Clark, P., Huybrechts, P., Joughin, I., 2005. Ice-sheet adn sea-level changes. Science 310, 456–460.

Banerjee, S. K., King, J., Marvin, J., 1981. A rapid method for magnetic granulometry with applications to environmental studies. Geophys. Res. Lett. 8, 333–336.

Cook, C., van de Flierdt, T., Williams, T., Hemming, S., Iwai, M., Kobayashi, M., Jimenez-Espejo, F., Escutia, C., González, J., Khim, B., McKay, R., Passchier, S., Bohaty, S., Riesselman, C., Tauxe, L., Sugisaki, S., Lopez Galindo, A., Patterson, M., Sangiorgi, F., Pierce, E., Brinkhuis, H., Scientists, I. E. ., 2013. Dynamic behavior of the East Antarctic ice sheet during Pliocene warmth. Nature Geoscience 6, 765–769.

Craw, D., Findlay, R., 1984. Hydrothermal alteration of Lower Ordivician granitoids and Devonian Beacon Sandstone at Taylor Glacier, McMurdo Sound, Antarctica. New Zealand Jour. Geol. Geophys. 27, 465–475.

Damaske, D., Ferraccioli, F., Bozzo, E., 2003. Aeromagnetic anomaly investigations along the Antarctic coast between Yule Bay and Mertz Glacier. Terra Antarctica 10, 85–96.

Dunlea, A., Murray, R., Harris, R., Vasiliev, M., Evans, H., Spivack, A., D'Hondt, S., 2013. Assessment and use of NGR instrumentation on the JOIDES Resolution to quantify U, Th, and K concentrations in marine sediment. Scientific Drilling 15, 57–63.

Dymond, J., Suess, E., Lyle, M., 1992. Barium in deep-sea sediment: A geochemical proxy for paleoproductivity. Paleoceanography 7, 163–181.

Escutia, C., Brinkhuis, H., Klaus, A., Expedition 318 Scientists, ., 2011. Wilkes Land glacial history: Expedition 318 of the riserless drilling platform Wellington, New Zealand, to Hobart, Australia Sites U1355- U1361, 3 January - 8 March 2010. Vol. 318 of Proc. IODP. Integrated Ocean Drilling Program Management International, Inc., Tokyo.

Ferraccioli, F., Armadillo, E., Jordan, T., Bozzo, E., Corr, H., 2009. Aeromagnetic exploration over the East Antarctic Ice Sheet: A new view of the Wilkes Subglacial Basin. Tectonophysics 478, 62–77.

Finn, C., Goodge, J., Damaske, D., Fanning, C., 2006. Scouting craton's edge in paleo-Pacific Gondwana. Springer, Berlin, Ch. 4.1, pp. 165–174.

Fretwell, P., Pritchard, H., Vaughan, D., Bamber, J., Barrand, N., Bell, R., Bianchi, C., Bingham, R., Blankenship, D., Casassa, G., Catania, G., Callens, D., Conway, H., Cook, A., Corr, H., Damaske, D., Damm, V., Ferraccioli, F., Forsberg, R., Fujita, S., Gim, Y., Gogineni, P., Griggs, J., Hindmarsh, R., Holmlund, P., Holt, J., Jacobel, R., Jenkins, A., Jokat, W., Jordan, T., King, E., Kohler, J., Krabill, W., Riger-Kusk, M., Langely, K., Leitchenkov, G., Leuschen, C., Luyendyk, B., Matsuoka, K., Mouginot, J., Nitsche, F., Nogi, Y., Nost, O., Popov, S., Tignot, E., Rippin, D., Rivera, A., Roberts, J., Ross, N., Siegert, M., Smith, A., Steinhage, D., Studinger, M., Sun, B., Tinto, B., Welch, B., Wilson, D., Young, D., Xiangbin, C., Zirizzotti, A., 2013. Bedmap2: improved ice bed, surface and thickness datasets for Antarctica. The Cryosphere 7, 375–393.

Gradstein, F., Ogg, J., Smith, A., 2004. Geologic Time Scale 2004. Cambridge University Press, Cambridge.

Gregory, J., Huybrechts, P., Raper, S., 2004. Threatened loss of hte Greenland ice-sheet. Nature 428, 616.

Huybrechts, P., de Wolde, J., 1999. The dynamic response of the Greenland and Antarctic Ice Sheets to Multiple-century climatic warming. J. Climate 12, 2169–2188.

Keating, B., Sakai, H., 1991. Amery Group red beds in Prydz Bay, Antarctica. Proc. ODP, Scientific Results 119, 795–809.

King, J. W., Banerjee, S. K., Marvin, J., 1983. A new rock magnetic approach to selecting sediments for geomagnetic paleointensity studies: application to paleointensity for the last 4000 years. Jour. Geophys. Res. 88, 5911–5921.

Lawrence, K. P., Tauxe, L., Staudigel, H., Constable, C., Koppers, A., McIntosh, W. C., Johnson, C. L., 2009. Paleomagnetic field properties near the southern hemisphere tangent cylinder. Geochem. Geophys. Geosyst. 10, Q01005.

Lisiecki, L., Raymo, M. E., 2005. A pliocene-Pleistocene stack of 57 globally distributed benthic δ^{18}O records. Paleoceanography 20 (PA1003).

Lowrie, W., 1990. Identification of ferromagnetic minerals in a rock by coercivity and unblocking temperature properties. Geophys. Res. Lett. 17, 159–162.

Lythe, M., Vaughan, D., Consortium, B., 2001. BEDMAP: A new ice thickness and subglacial topgrahic model of Antarctica. Jour. Geophys. Res. 106, 11,335–11,351.

Maher, B. A., Thompson, R., 1999. Quaternary Climates, Environments and Magnetism. Cambridge University Press.

Mawson, D., 1915. The home of the Blizzard. Vol. 2. William Heinemann, London.

Mikhalsky, E., Sheraton, J., Laiba, A., Tingey, R., Thost, D., Kamenev, E., Fedorov, L., 2001. Geology of the Pince Charles Mountains, Antarctica. Geoscience Australia Bulletin 247, 226p.

Miller, K., Wright, J., Browning, J., Kulpecz, A., Kominz, M., Naish, T., Cramer, B., Rosenthal, Y., Peltier, W., Sosdian, S., 2012. High tide of the warm Pliocene: Implications of global sea level for Antarctic deglaciation. Geology 40, 407–410.

Pagani, M., Liu, Z., LaRiviere, J., Ravelo, A., 2010. High Earth-system climate sensitivity determined from Pliocene carbon dioxide concentraions. Nature Geoscience 3, 27–30.

Patterson, M., McKay, R., Naish, T., Escutia, C., Jimenez-Espejo, F., Raymo, M. E., Tauxe, L., Brinkhuis, H., IODP Expedition 318 Scientists, 2014. Response of the East Antarctic Ice Sheet to orbital forcing during the Pliocene and early Pleistocene. Nature Geoscience 7, 841–847.

Schmidt, P., Williams, G., 2013. Anisotropy of thermoremanent magnetization of Cryogenian glaciogenic and Ediacaran red beds, South Australia: Neoproterozoic apparent of true polar wander? Global and Planetary Change 110, 289–301.

Schwehr, K., Tauxe, L., Driscoll, N., Lee, H., 2006. Detecting compaction disequilibrium with anisotropy of magnetic susceptibility. Geochem. Geophys. Geosyst. 7.

Tauxe, L., Bertram, H., Seberino, C., 2002. Physical interpretation of hysteresis loops: Micromagnetic modelling of fine particle magnetite. Geochem., Geophys., Geosyst. 3.

Tauxe, L., Butler, R., van der Voo, R., Banerjee, S., 2010. Essentials of Paleomagnetism. University of California Press, Berkeley.

Tauxe, L., Stickley, C., Sugisaki, S., Bijl, P., Bohaty, S., Brinkhuis, H., Escutia, C., Flores, J.-A., Houben, A., Iwai, M., Jimenez-Espejo, F., McKay, R., Passchier, S., Pross, J., Riesselman, C., Roehl, U., Sangiorgi, F., Welsh, K., Klaus, A., Fehr, J., Bendle, J., Dunbar, R., Gonzalez, S., Hayden, T., Katsuki, K., Olney, M., Pekar, S., Shrivastava, P., van de Flierdt, T., Williams, T., Yamane, M., 2012. Chronostratigraphic framework for the IODP Expedition 318 cores from the Wilkes Land Margin: constraints for paleoceanographic reconstruction. Paleoceanography 27.

Vaughan, D., Comiso, J., Allison, I., Carrasco, J., Kaser, G., Kwok, R., Mote, P., Murray, T., Paul, F., Ren, J., Rignot, E., Solomina, O., Steffen, K., Zhang, T., 2013. Observations: Cryosphere. Climate Change 2013: The Physical Science Basis. Contribution of Working Group I to the Fifth Assessment Report of the Intergovernmental Panel on Climate Change. Cambridge University Press, Cambridge.

Veevers, J., Saeed, A., 2011. Age and composition of Antarctic bedrock reflected by detrital zircons, erratics and recycled microfossils in the Prydz Bay-Wilkes Land-Ross Sea-Marie Byrd Land sector (70°-240°E). Gondwana Research 20, 710–738.

Williams, G., Gostin, V., McKirdy, D., Preiss, W., 2008. The Elatina glaciation, late Cryogenian (Marinoan Epoch), South Australia: Sedimentary facies and palaeoenvironments. Precambrian Research 163, 307–331.

Zachos, J., Pagani, M., Sloan, L., Thomas, E., Billups, K., 2001. Trends, rhythms and aberrations in global climate 65 Ma to present. Science 292, 686.

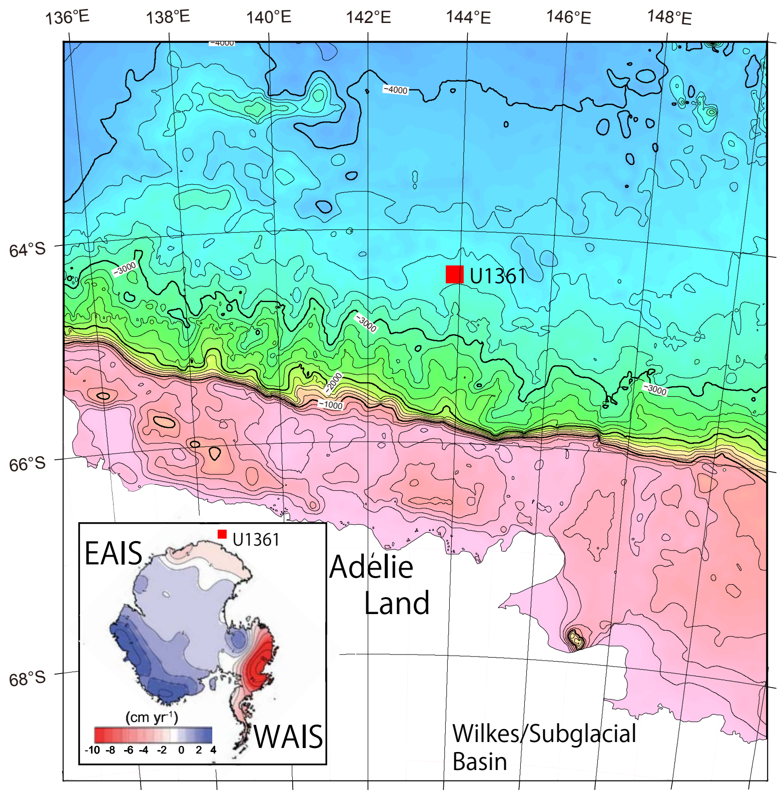

Figure 1: Map showing location of IODP Expedition 318 Site U1361 drilled at 64.2457°S, 143.5320°E, 3466 mbrf. Inset (adapted from the Vaughan et al. (2013)) shows the ice loss determined between 2006 and 2012 from GRACE time-variable gravity data in cm water/year from the East and West Antarctic Ice Sheets (EAIS and WAIS respectively).

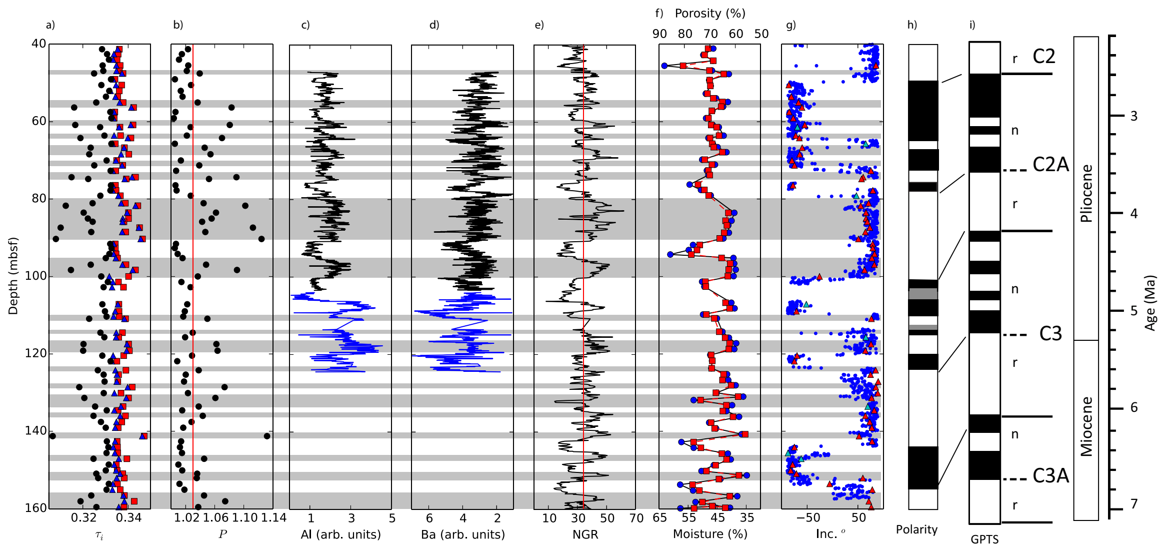

Figure 2: a) Eigenvalues (red squares: τ_1, blue triangles: τ_2, black circles: τ_3) b) Anisotropy degree, ($P = \tau_1/\tau_3$). c) Aluminum (expressed as arbitrary units from XRF data. d) Barium (arbitrary units), e) Natural gamma radiation (NGR, Escutia et al. (2011)). f) Shipboard moisture content and porosity from (Escutia et al., 2011). g) Inclinations from Tauxe et al. (2012). Small blue dots are data from the archive halves demagnetized to 20 mT. Red (cyan) triangles are acceptable best-fit lines and Fisher means respectively, according to the criteria defined by Tauxe et al. (2012). h) Polarity log. Black intervals are normal (negative inclinations) , white reverse (positive inclinations) and grey are intervals with no data. i) Geomagnetic Polarity Time Scale (GPTS), black (white) intervals are normal (reverse) polarity. Chrons are calibrated by as in the Geological Time Scale of Gradstein et al. (2004), GTS04 for consistency with other work on Expedition 318 material. Intervals with high P ($P > 1.03$) are marked with grey bars. Black lines in barium and aluminum data are from Cook et al. (2013) and blue lines are reported here.

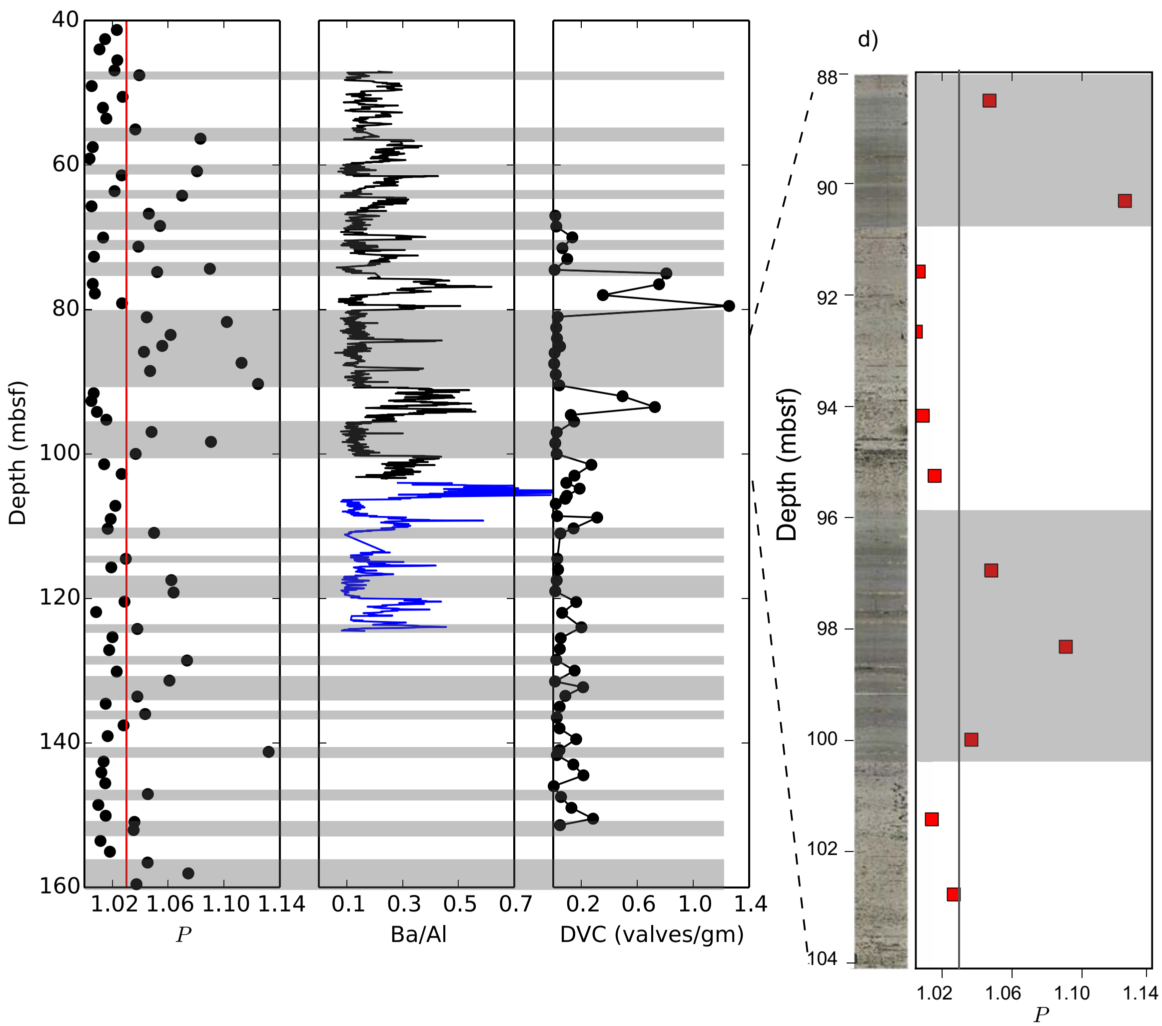

Figure 3: a) P (from Fig. 2). Grey bars as in Fig. 2. d) Ba/Al (data from Fig. 2.) c) Diatom valve concentration (valves/g; black). Valve counts (from Cook et al. (2013)) are divided by 10^7. d) Expanded section showing core photo and associated P values.

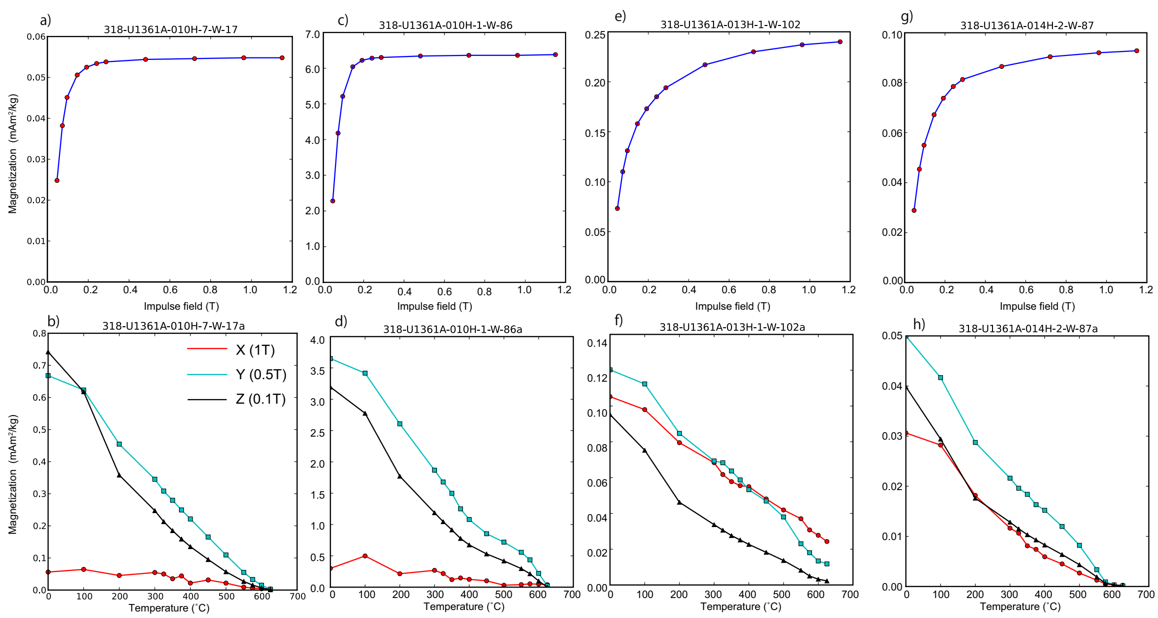

Figure 4: a), c), e), g) Representative isothermal remanent magnetization (IRM) acquisition curves. b), d), f), h) 3-D IRM demagnetization experiments.

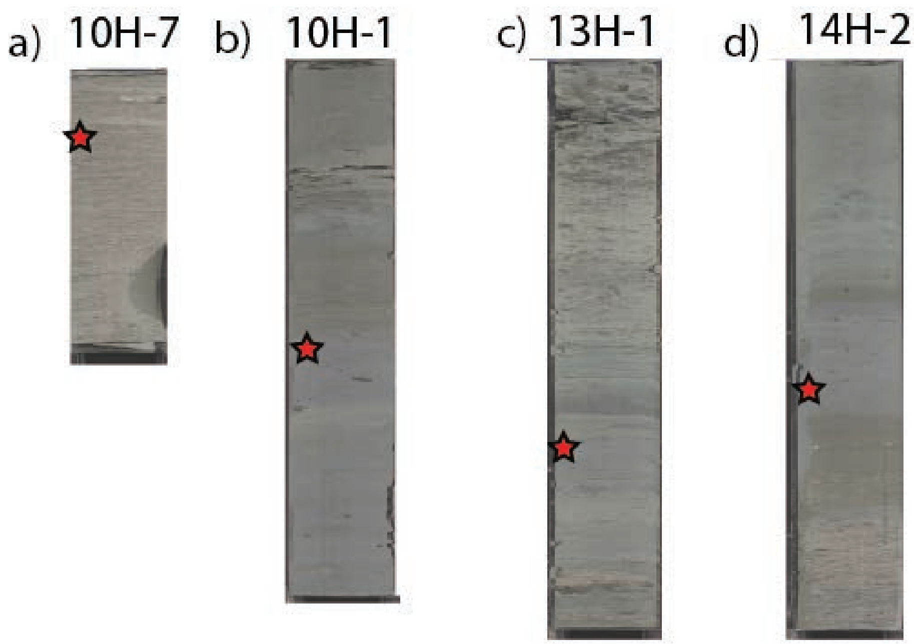

Figure 5: Photos of the core sections in which the samples in Figure 4 were taken. Locations of sample horizons indicated by red stars. Exposure of the photos enhanced to 100%, but colors were otherwise not manipulated. Horizontal scale 2x vertical. Section lengths are 74cm in a) and 150cm in b-d.

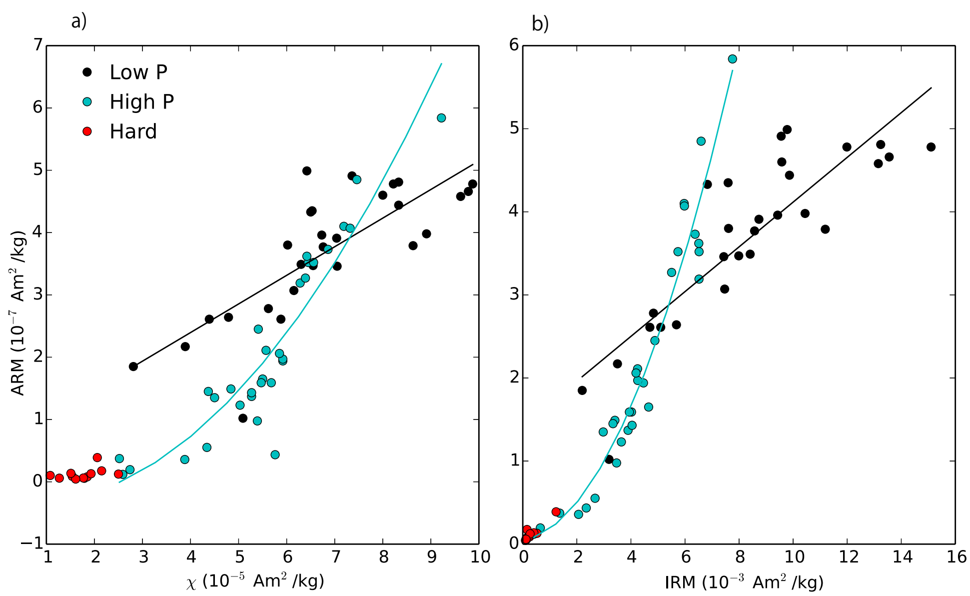

Figure 6: a) Plot of mass normalized ARM versus bulk susceptibility (χ) for the three types of specimens. Best-fit lines from a linear regression for the high P versus low P groups of low $\mathrm{IRM}_{0.5T}^{1.0T}$ specimens are also shown, suggesting that the high P (clay-rich) sediments have smaller magnetic grain sizes as well as bulk sediment grain sizes. b) Plot of mass normalized ARM versus IRM distinguished by different degrees of anisotropy (P) and magnetic 'hardness' ($\mathrm{IRM}_{0.5T}^{1.0T}$). Best-fit line and second order polynomial are shown for the low and high P groups respectively.

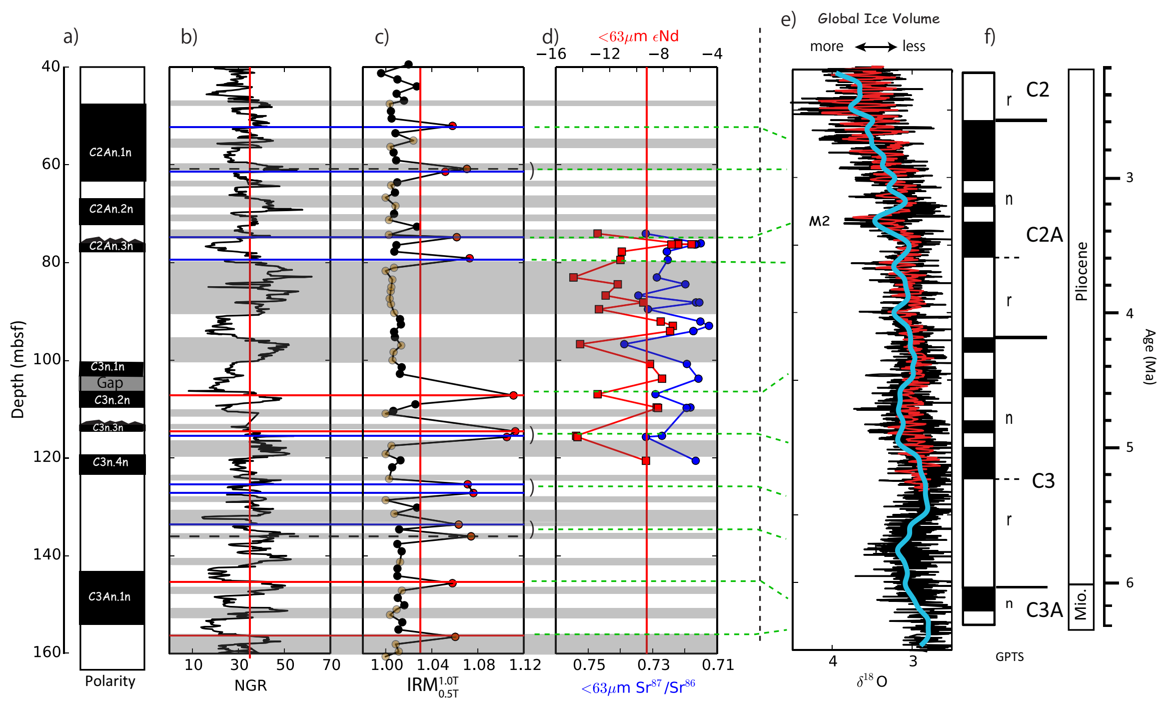

Figure 7: Summary of data for U1361A. a) Magnetic polarity zonation (see Fig.1), b) NGR (Fig. 2), c) $\mathrm{IRM}^{1.0T}_{0.5T}$ where black dots are 'magnetite', brown are 'maghemite' and red are 'hard', d) ϵNd and $^{87}Sr/^{86}Sr$ (Cook et al., 2013), e) Global stacks of oxygen isotopes of Zachos et al. (2001) (black) and Lisiecki and Raymo (2005) (red). Heavy cyan curve is a low pass filter of the Zachos et al. (2001) curve. f) The GPTS (Gradstein et al., 2004). The grey intervals represent high anisotropy layers from Fig. 1. Horizontal lines are the positions of high $\mathrm{IRM}^{1.0T}_{0.5T}$ samples. Blue (red) solid lines are low clay to high clay (high clay to low clay) transitions. Black dashed lines are neither. Green dashed lines are correlations of high $\mathrm{IRM}^{1.0T}_{0.5T}$ layers to the oxygen isotopic record.

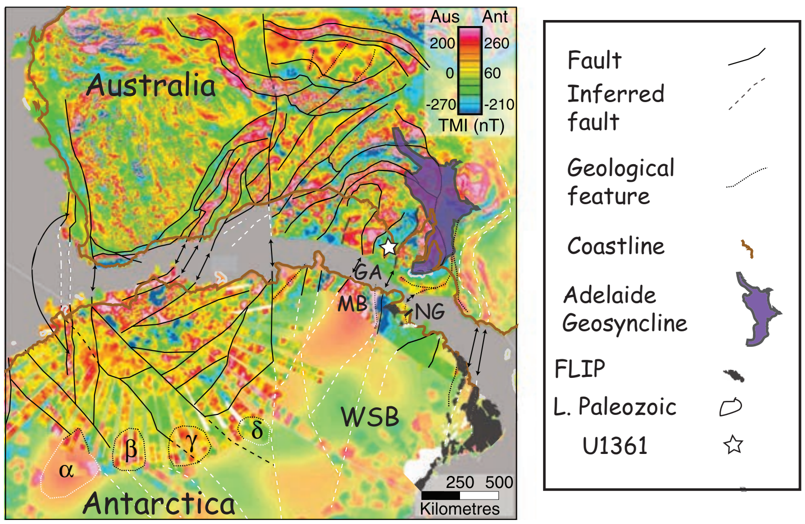

Figure 8: Magnetic anomaly map (for Australia and Wilkes Land region of Antarctica of Aitken et al. (2014). The continents are in the 'Leeuwen' Gondwana reconstruction for 160 Ma. The location of Site U1361 is the current location with respect to Antarctica. WSB is the Wilkes Subglacial Basin. Geological piercing points drawn as double arrows are suggested geological correlations. GA is the Gawler-Terre Adélie connection. Geological units of Ferrar Large Igneous Province (FLIP) (black) and Lower Paleozoic age (white) were inferred from isotopic analyses of Cook et al. (2013) as sources of detritus in the clay-rich and clay-poor zones. The closest likely source of the Lower Paleozoic age material is just south of the Ninnis Glacier (NG). The closest likely source of FLIP material is in the WSB where it is inferred to exist based on aeromagnetic anomalies of Damaske et al. (2003) and Ferraccioli et al. (2009). It is possible that there are outcrops of hydrothermally altered Beacon sandstones (with hematite enrichment) in association with the FLIP material, as seen in near the Taylor Glacier Craw and Findlay (1984). Alternatively, the Adelaide geosyncline of South Australia from Schmidt and Williams (2013) contains outcrops of the red beds of the Elatina Formation. If present on the Antarctic continent, these units could be the source of the hematite present at many clay-rich/clay-poor transitions.

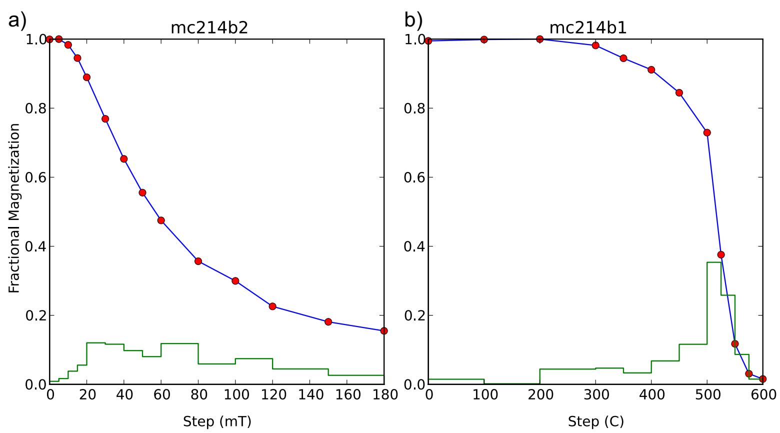

Figure 9: Typical example of high coercivity behavior coupled with blocking temperatures (maximum of ∼580°C) typical of magnetite for a specimen from the McMurdo Sound volcanics. a) Alternating field demagnetization. b) Thermal demagnetization. [Data from Lawrence et al. (2009) available for download at: http://earthref.org/MAGIC/9411/.]

*Highlights (for review)

- Climate models predict growth of East Antarctic Ice Sheet with global warming
- Records from IODP Exp. 318 show instability of the EAIS during the Pliocene.
- Rock magnetic techniques detect erosion of three distinct geological units.

Figure 1
Click here to download Figure: map.eps

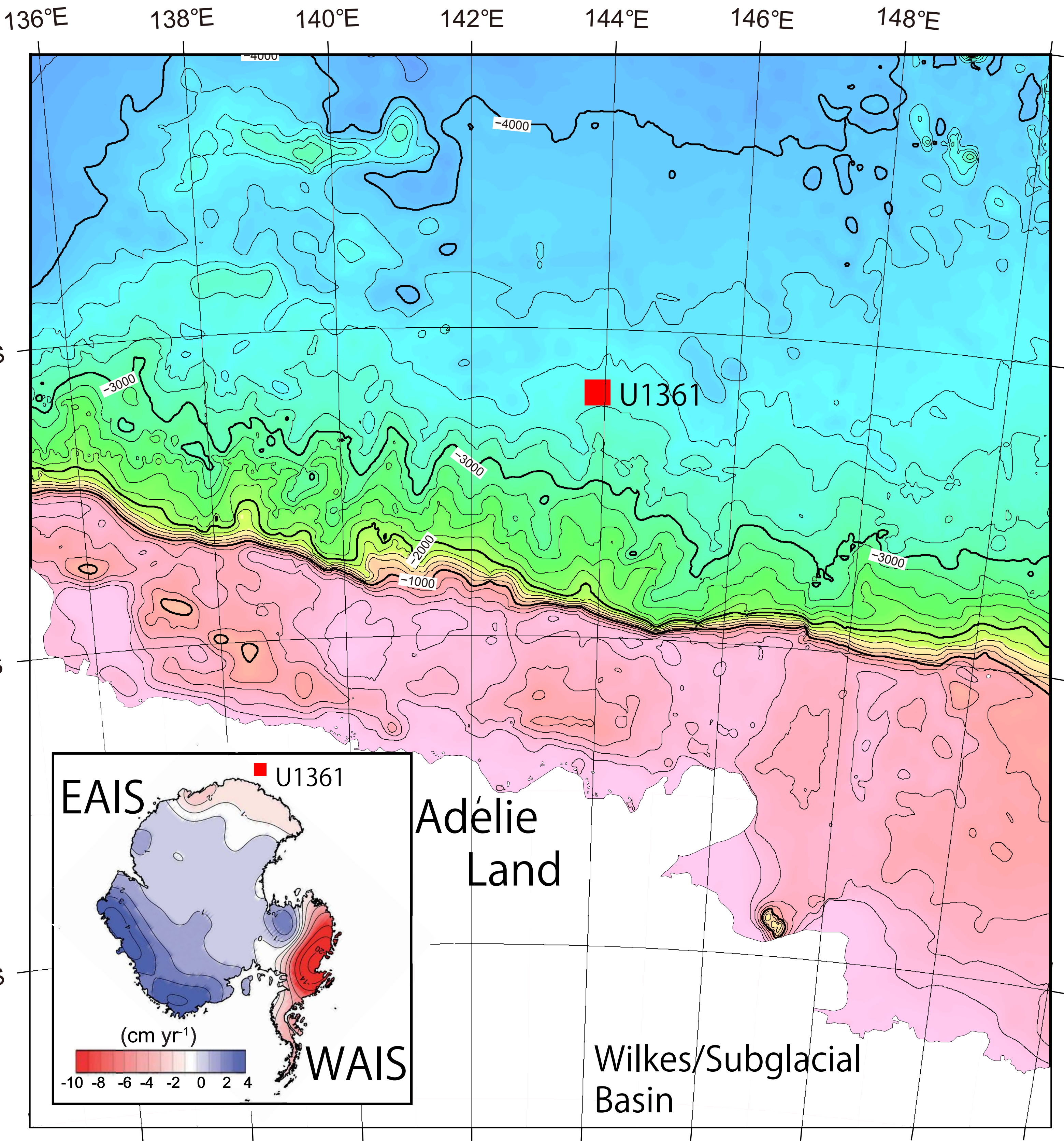

Figure 2

Click here to download Figure: AMS.eps

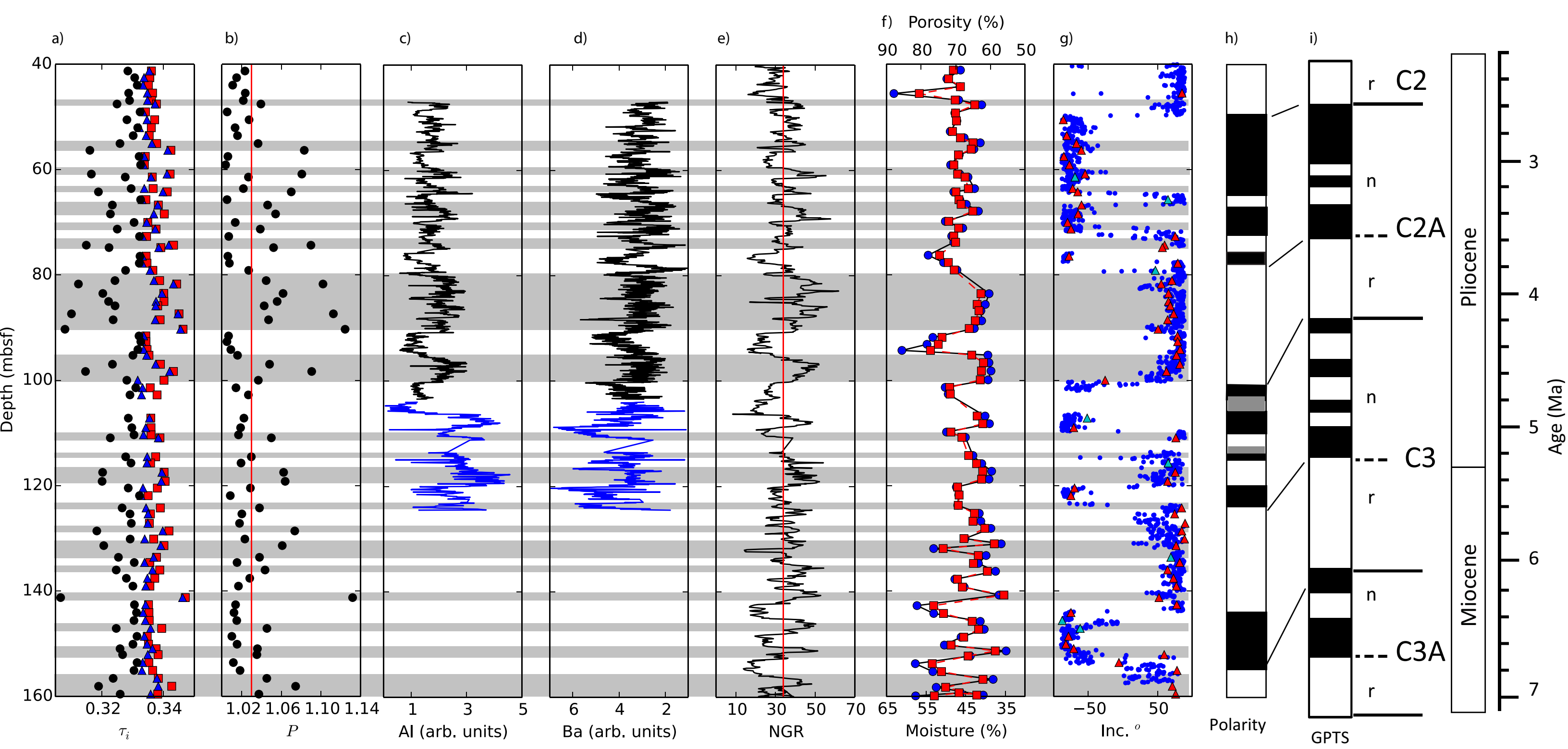

Figure 3
Click here to download Figure: P_Prod.eps

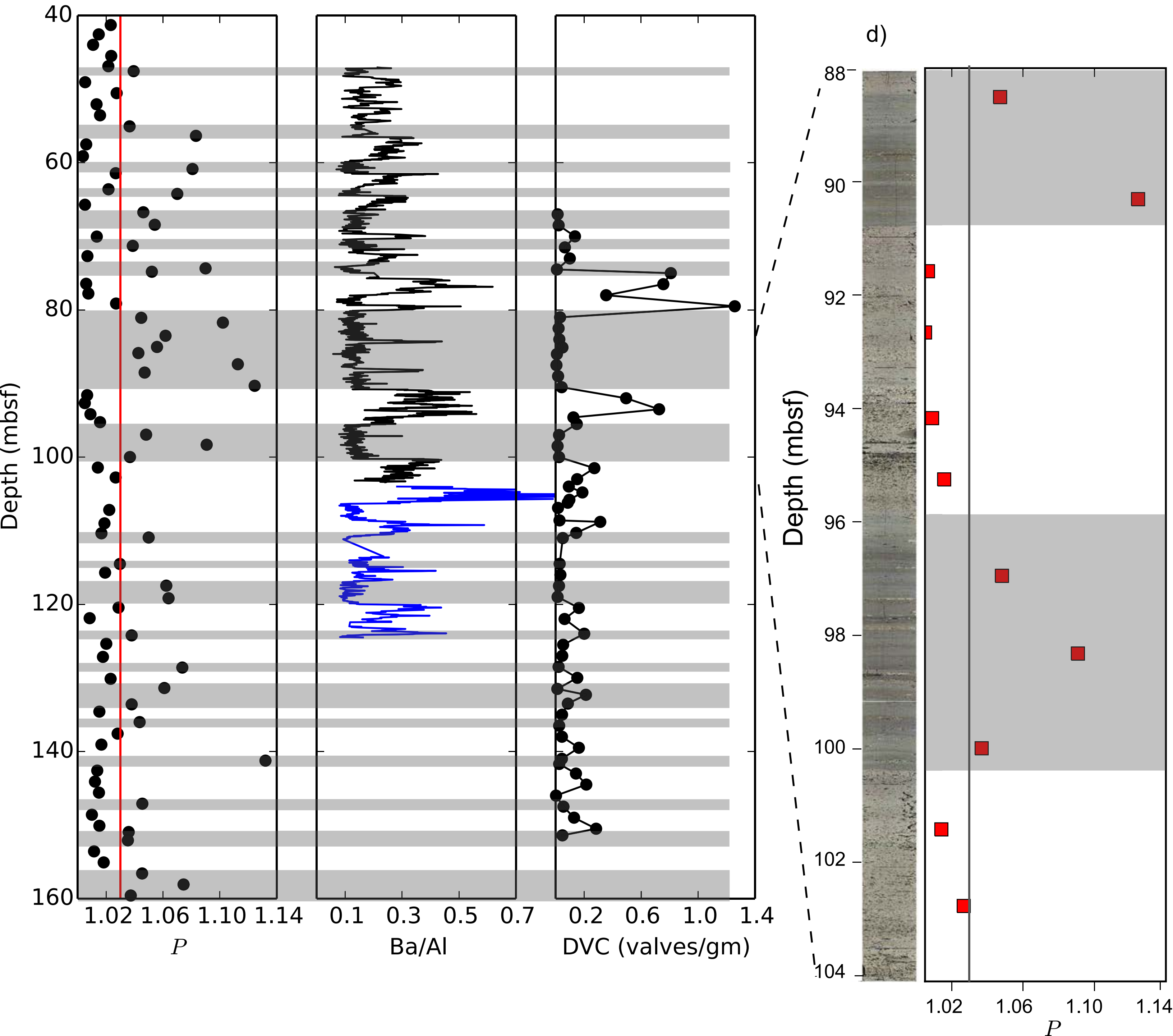

Figure4

Click here to download Figure: Hs_Hfrac.eps

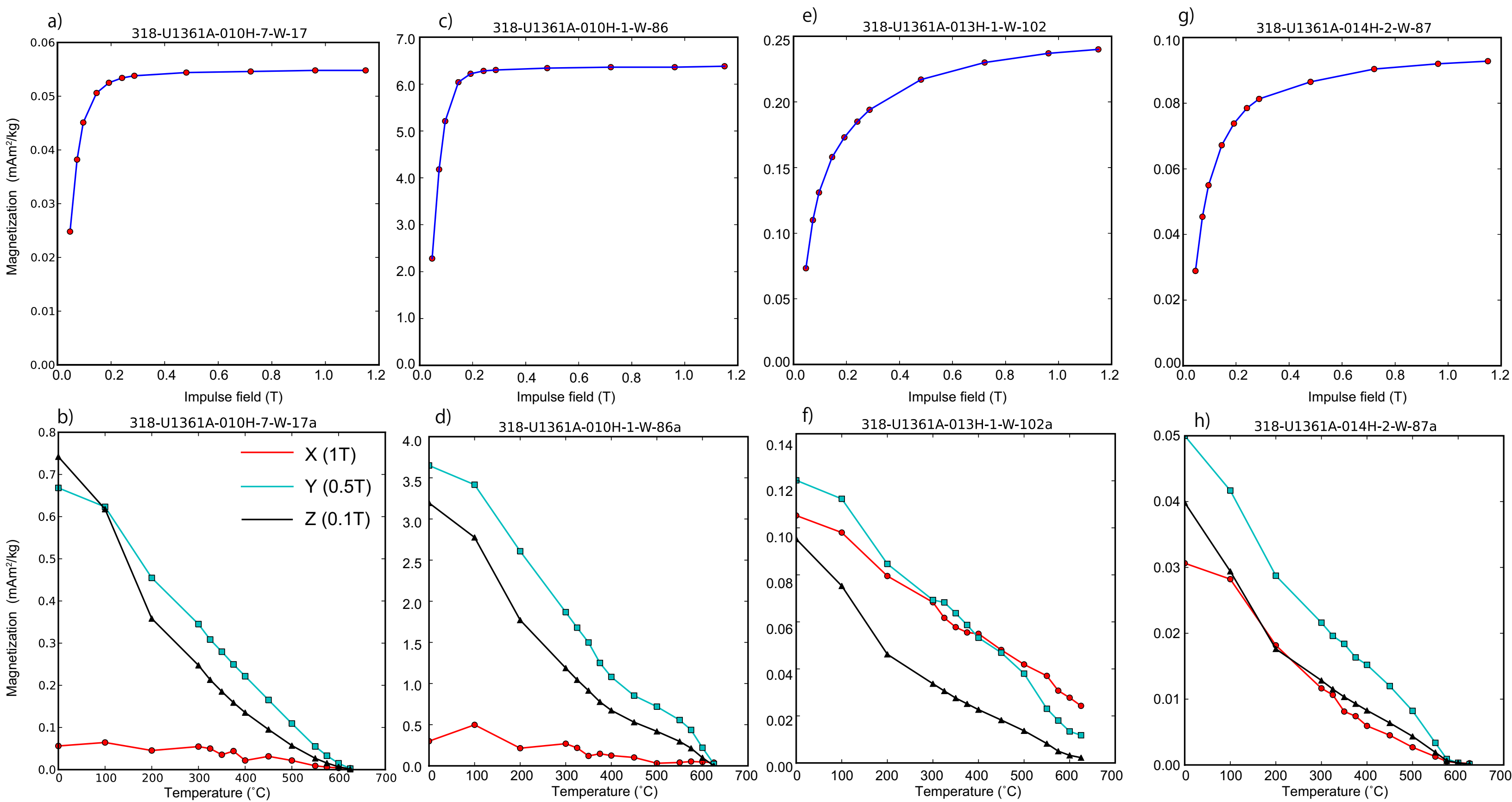

Figure 5
Click here to download Figure: corephotos.eps

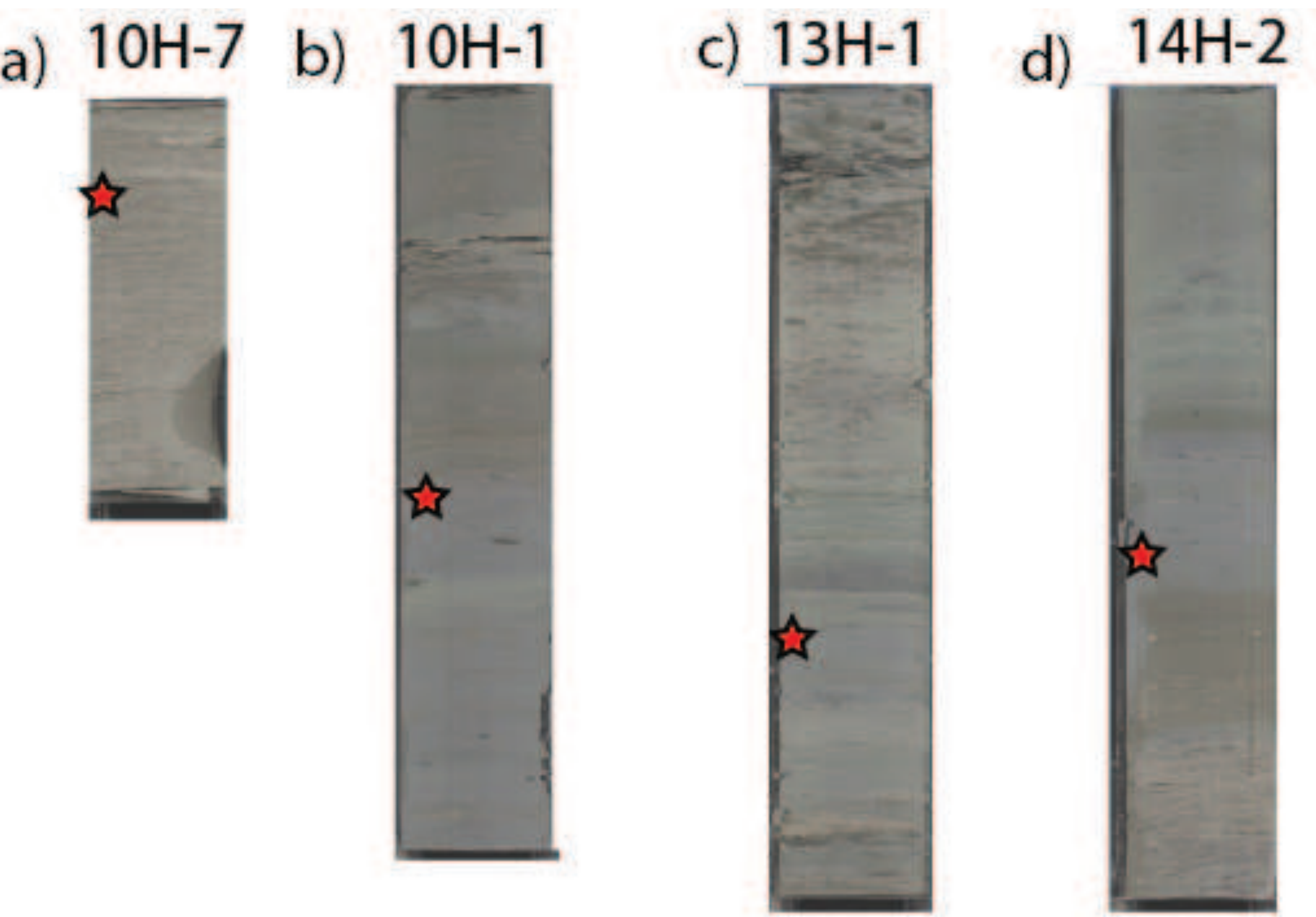

Figure 6
Click here to download Figure: RmRms.eps

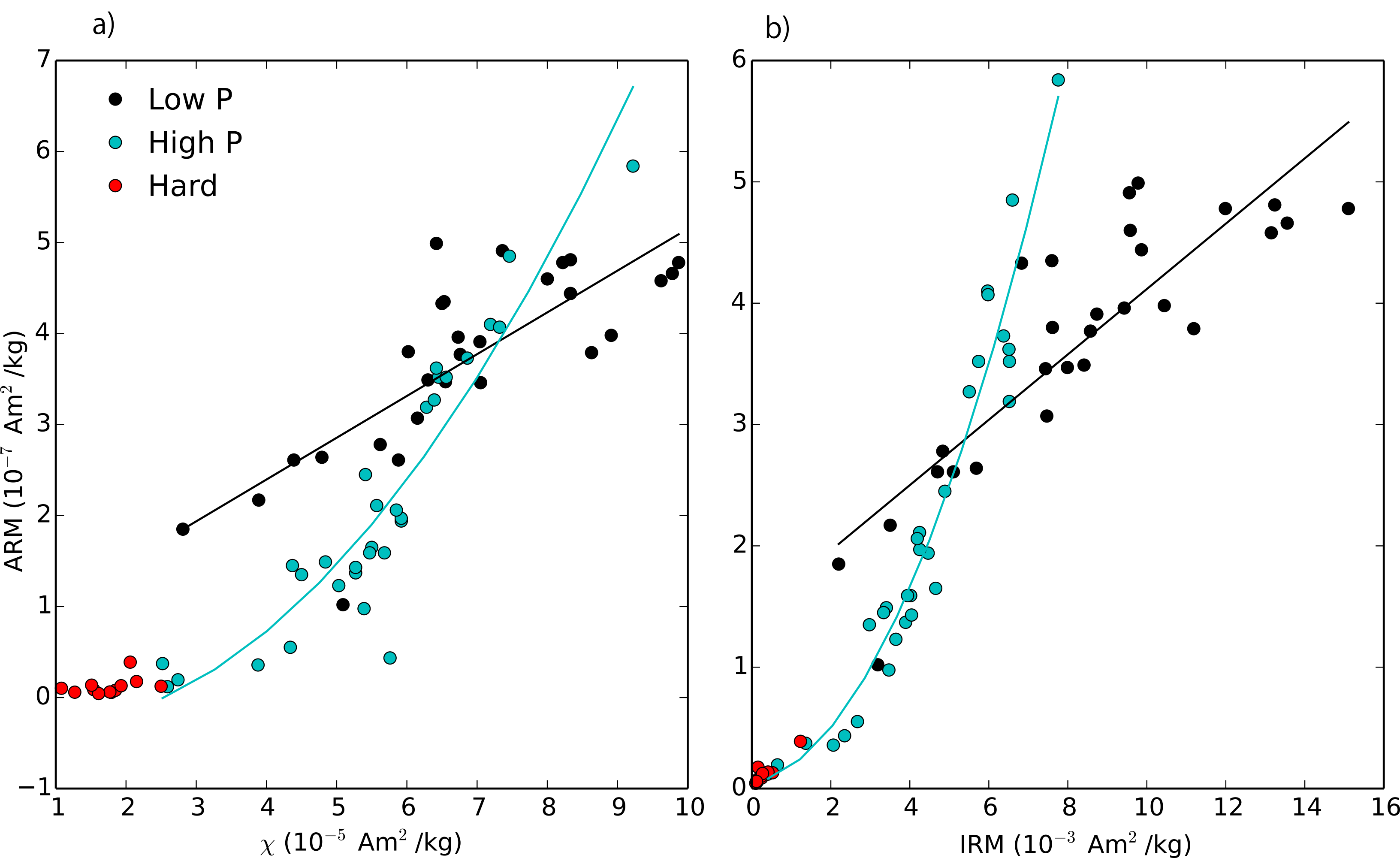

Figure 7

Click here to download Figure: Results_with_LR04.eps

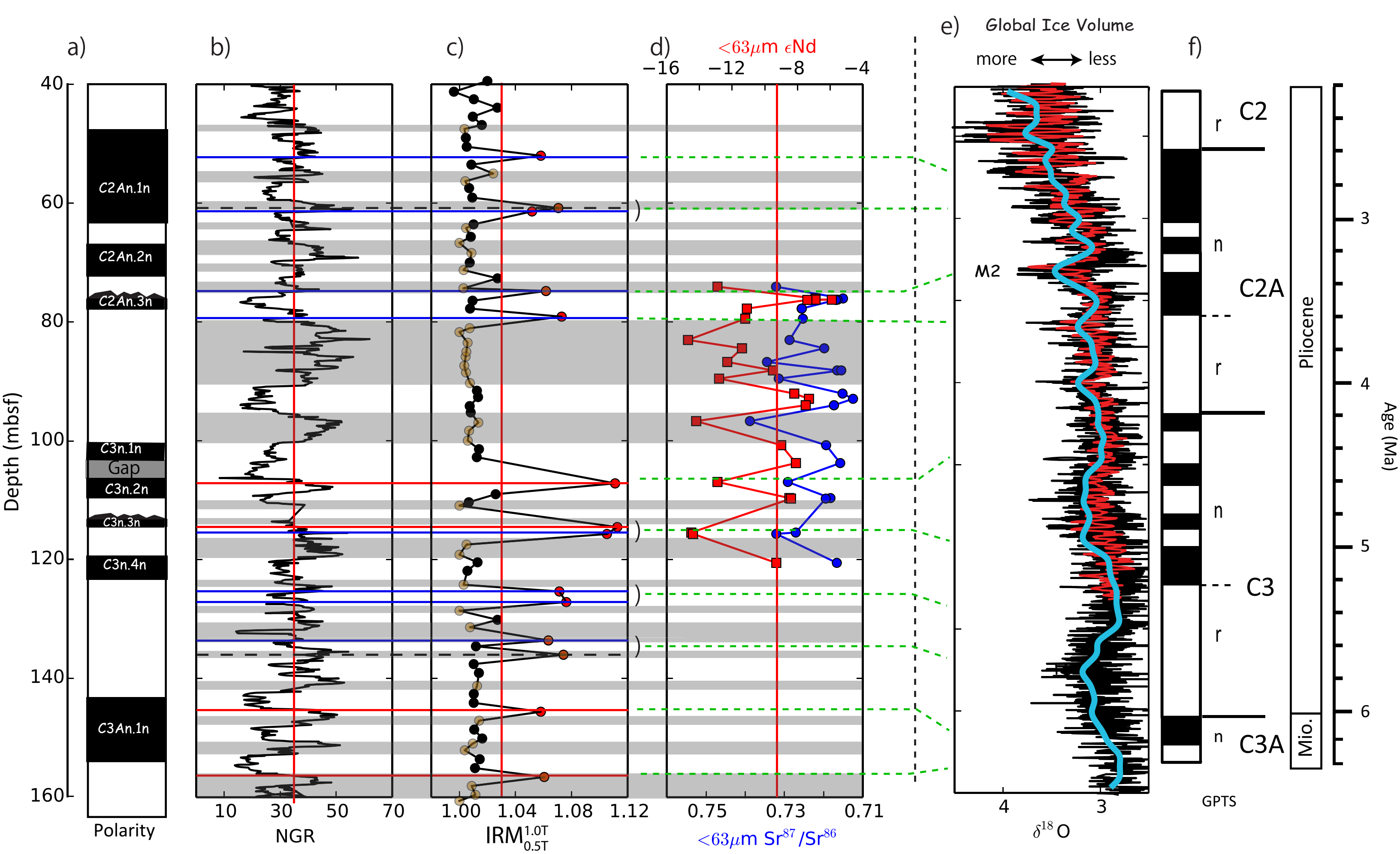

Figure 8
Click here to download Figure: maganom.eps

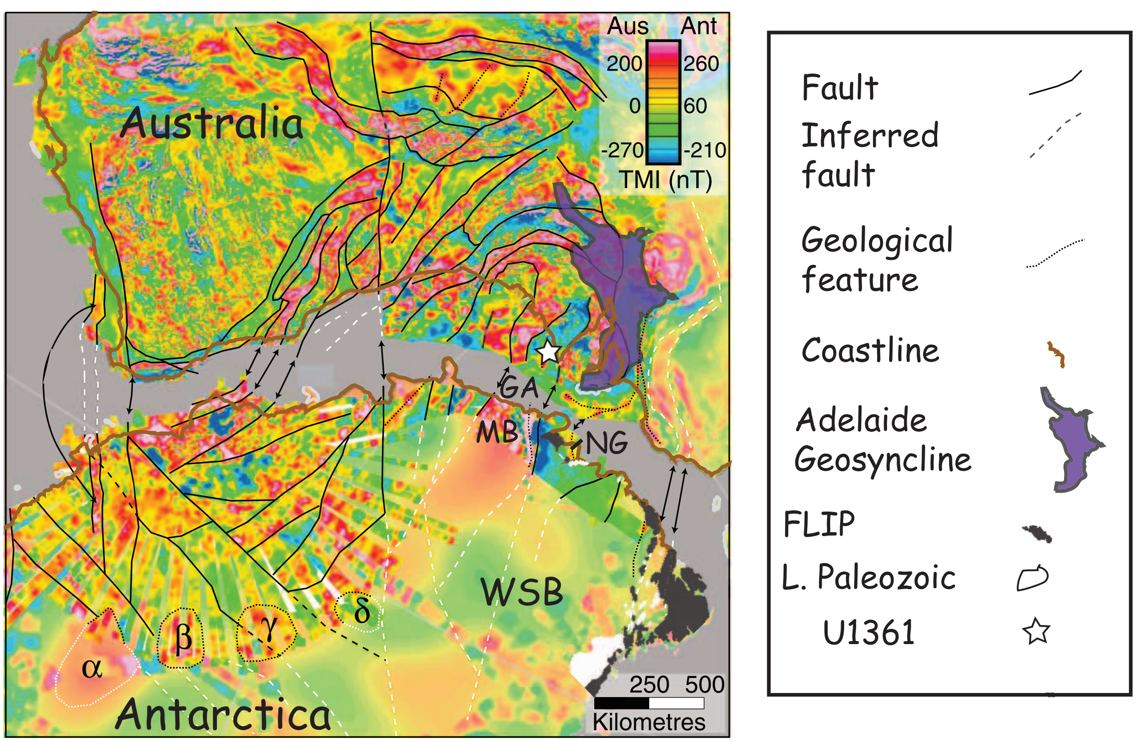

Figure 9

Click here to download Figure: McMurdo_mc_hard_Low_Tb.eps

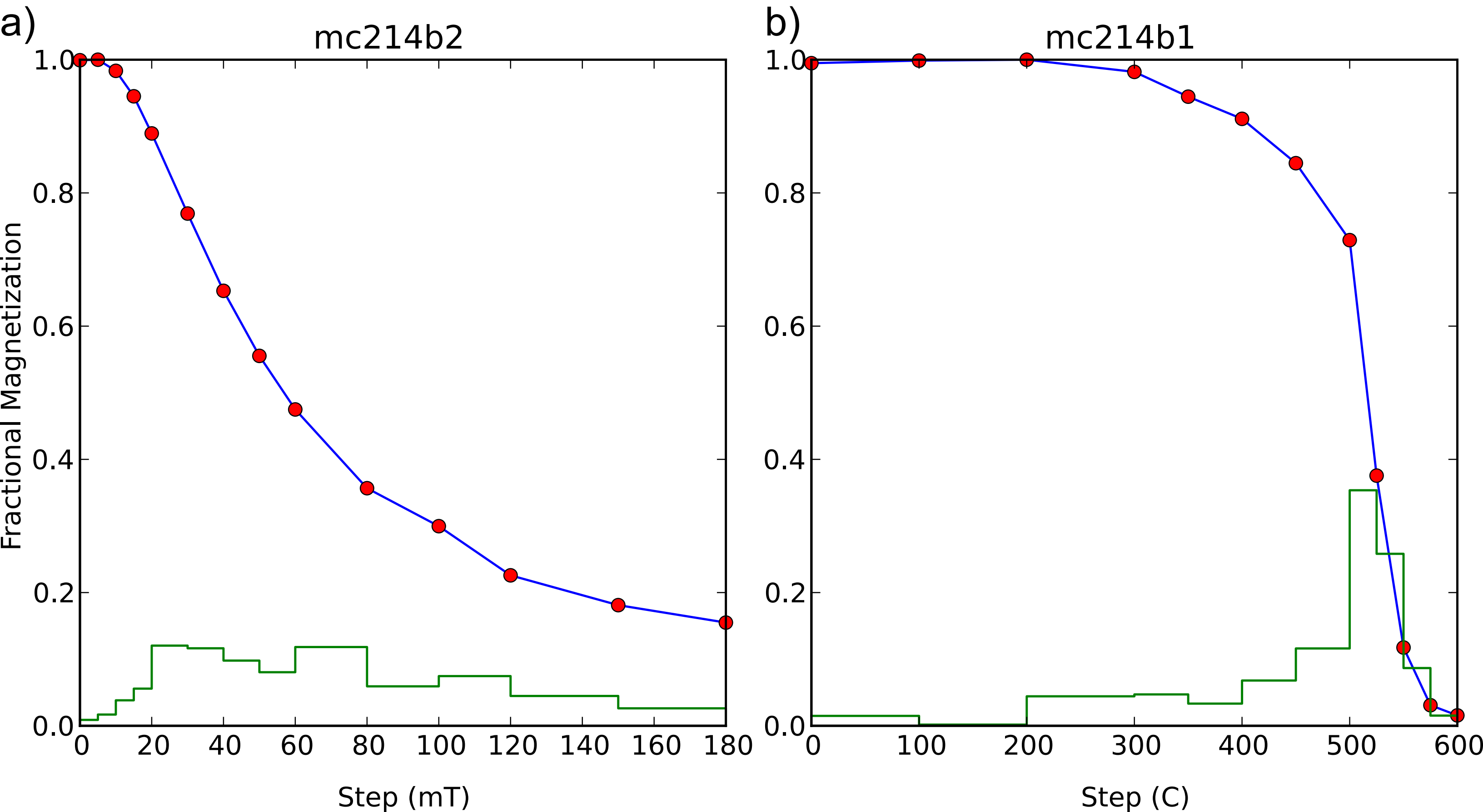

LaTeX Source Files

Click here to download LaTeX Source Files: U1361A_AMS_2.0.tex